AERODYNAMIC AND AEROELASTIC EXPERIMENTAL INVESTIGATION ON THE PROPAGATION OF INLET TEMPERATURE DISTORTIONS IN A LOW PRESSURE TURBINE STAGE

L. Simonassi – M. Zenz – S. Pramstrahler – P. Bruckner – F. Heitmeir – A. Marn

Institute of Thermal Turbomachinery and Machine Dynamics, Graz University of Technology, Graz, Austria. Email: loris.simonassi@tugraz.at

ABSTRACT

The inlet conditions of modern low pressure turbine (LPT) present significant flow non-homogeneities, which can have direct consequences on both its aerodynamic performance and vibrations. The rise in turbine entry temperatures and pressure ratios needed to achieve higher efficiencies and power output requires an increase of cooling and purge flow injections, leading to the generation of strong temperature distortions at the inlet of the LPT. Additionally, the stronger interaction between engine components due to the drastic decrease of axial spacing and to the reduction of the stage count facilitates the propagation of circumferential distortions of total pressure and temperature.

This paper reports on the results of an experimental investigation focused on total temperature distortions at the inlet of a modern low pressure turbine stage and on the propagation of such inflow disturbances through the stage, with a particular focus on both the aerodynamic and aero-elastic performance of the turbine. The measurement activity was carried out in a one and a half stage subsonic turbine test facility at the Institute of Thermal Turbomachinery and Machine Dynamics at Graz University of Technology at an engine relevant operating condition. Total temperature distortions with different intensities were generated upstream of the stage through the localised injection of air at different mass flow and temperature, ranging from 30% to 130% of the nominal inlet temperature. A setup with clean inflow was additionally used as reference. Aerodynamic measurements were taken upstream of the investigated stage by means of a five-hole-probe (5HP). The rotor blade vibration data was acquired with strain gauges applied on different blades, in combination with a telemetry system.

The rotor vibrations were influenced by the alterations created by the circumferential temperature perturbation in the flow. In particular, the temperature of the distortion was found to influence directly the amplitude of the rotor blade forced response. Therefore, important aerodynamic and aero-elastic effects were linked to the presence of total temperature distortions in the inlet flow field of an LPT stage.

KEYWORDS

AEROELASTICITY, LOW PRESSURE TURBINES, INLET DISTORTIONS, FORCED RESPONSE, STRAIN GAUGES.

NOMENCLATURE

Abbreviations

EF	Eigenfrequency	STTF-AIAA	Subsonic Test Turbine Facility for Aerodynamic, Aeroelastic and Acoustic Investigations
EO	Engine order		
SG	Strain gauge		
IGV	Inlet guide vane	TEC	Turbine Exit Casing
LPT	Low pressure turbine	5HP	Five-holes-probe

Greek

α	Yaw angle
γ	Pitch angle
ρ	Density

Symbols

Ma	Mach number	Pt	Total pressure
P	Pressure	T_j	Temperature of the injection
		$\dot{m}_j$	Injected mass flow

INTRODUCTION

The design of modern aero engines is aimed at achieving high efficiency and low weight, in order to reduce fuel consumption and therefore CO2 emissions. The use of lighter materials and the down-sizing of the components is crucial to achieve these goals. A disadvantage of reducing axial distances between engine components is the propagation of circumferential distortions of total pressure and temperature through the machine. This disturbances propagating from the combustion chamber or from the upstream stages cause direct consequences on turbomachinery performances.

Early experimental studies on the effects of inlet flow distortion in turbine rows were done by (Munk & Prim, 1947). (Schwab, et al., 1983) studied the modifications of performance in an axial turbine stage under the influence of radial non-uniform inlet temperature profile. The results of an experimental campaign carried out in a large-scale low speed axial turbine presented by (Butler, et al., 1989) demonstrated the increase of secondary flows due to temperature gradients originating from temperature distortions propagating from the turbine inlet. The influence of realistic turbine non-uniform inlet conditions on secondary flows was investigated also analytically (Lakshminarayana, 1975) and computationally by (Hermanson & Thole, 2002), who highlighted the need to consider realistic stage inlet profiles, due to the influence of pressure and temperature gradients on the secondary flows intensity.

Detailed analysis of the mechanisms that drive temperature disturbances transport through a turbine stage were presented by (Gaetani, et al., 2019). (Ong & Miller, 2012) also studied the effects on the secondary flows production driven by the combination of thermal gradients and blade row interactions.

Forced response measurements related to the excitation due to turbine inlet temperature distortions are sparse. (Manwaring & Kirkeng, 1997) attempted to predict the effect of temperature distortions on LPT blades based on the temperature profiles measured downstream of the HPT. The study suggested that the analysis of blade vibrations response to turbine inlet flow variations need to be implemented in the design process. Further, the aeromechanical effect of temperature non-uniformities with interest on rotor blade excitation was investigated by (Breard, et al., 2003) using 3D full-annulus simulations. This study concluded that the total blade excitation forcing can be modified substantially when the effects of temperature distortion are considered.

Previous forced response measurements were carried out in the subsonic test turbine facility of the Institute of Thermal Turbomachinery and Machine Dynamics of Graz University of Technology. In particular, a study dealing with the influence of total pressure inflow inhomogeneity on the vibratory response of low pressure turbine rotor blades was presented in (Simonassi, et al., 2019). Moreover, the impact of the azimuthal position of the total pressure inflow distortion relative to the stator vanes on the propagation of the flow disturbances through a low pressure turbine stage and on the resulting rotor blade vibratory response was analysed by the same authors in (Simonassi, et al., 2020).

The present work presents the results of an experimental investigation focused on the propagation of temperature inflow distortions through a modern low pressure turbine stage, with a particular focus on both the aerodynamic and aero-elastic characteristics of the turbine.

EXPERIMENTAL METHODOLOGY AND TEMPERATURE DISTORTION

Subsonic Test Turbine Facility

The cross section of the Subsonic-Test-Turbine-Facility for Aerodynamic, Acoustic and Aeroelastic Investigations located at the Institute of Thermal Turbomachinery and Machine Dynamics of the Graz University of Technology is shown in Figure 1. The facility relies on a 3MW compressor station for the supply of compressed air. The inlet air flows through a de-swirler, a perforated metal plate and a set of inlet guide vanes (IGVs) before reaching the stage inlet. This guarantees well-defined and uniform conditions at the stage inlet. The tested LPT stage is representative of the last stage of a commercial engine and consists of a stator row and a high aspect ratio unshrouded rotor. The aerodynamic design of the low pressure turbine stage was performed by MTU Aero Engines. The turbine diameter is approximately half of that of a commercial aero engine LPT. The influence of potential effects on the blade vibration measurements was reduced to a minimum by installing a vane-less TEC downstream of the rotor row. An extensive description of the test facility is given in (Moser, et al., 2007). The main geometrical details and the blade and vane count are reported in Table 1.

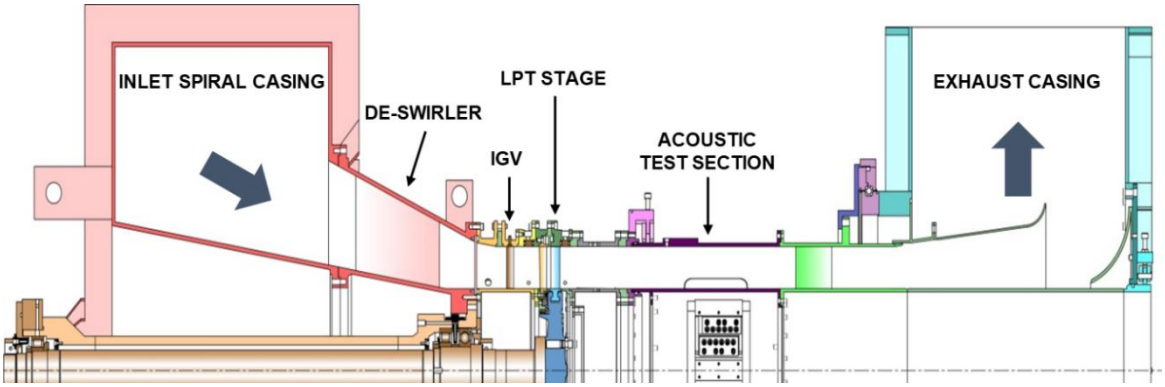

Figure 1: Cross-section of the subsonic test facility. STTF – AIAA.

Table 1: Details of the stage geometry.

Geometry details	
IGV/Stator/Rotor (vanes/blades number)	83/96/72
Vane-less TEC	-
Tip gap/Blade height	1%
Hub/Tip	2/3

Table 2: Operating conditions.

Nominal operating conditions	
Stage pressure ratio	1.16
Reduced speed	2999 rpm
Reduced mass flow	6.82 kg/s
Inlet total temperature	348.65 K (75.5°C)

Operating Conditions

In order to study the effect of the temperature inlet distortion on the rotor flow field and on the rotor vibrations, both the aerodynamic measurements and the blade vibration data were acquired at a stable operating point. Table 2 groups the reduced speed, reduced mass flow (both referred to 288.15 K and 1013.25 mbar) and pressure ratio of this operating point.

Temperature Distortion Generation

Principle

The aim of the temperature distortion generator is to create a localised total temperature distortion in the inlet flow field of the LPT stage under investigation (STTF_AIAA). In order to create an even temperature distortion along the span, the distortion generator was designed to be as high as the flow channel and 7 equally spaced air pipes were used along the injector height. 4 injectors were built and to be fitted in the machine contemporary to achieve 4 distortions along the circumference in the inlet plane. The air injection system can provide and injection of air at a temperature ranging from 298 K to 373 K, equal to 85.5% to 107.2% of the mean undisturbed inlet flow temperature. Therefore, both positive ($T_j > T_{0,avg}$) and negative ($T_j < T_{0,avg}$) total temperature distortion can be generated with this system.

Injector Design

A schematic cross-section of the injector is shown in Figure 2. The air is processed by the heating system (used to precisely regulate the injection temperature and mass flow) and is then divided between the 7 pipes to generate a homogeneous injection in radial direction. A thermocouple and a static pressure tap are mounted in the air supply line just before the air is divided and fed to the injector.

In addition, the injector body is equipped with 9 measuring heads to allow the measurement of total pressure and total temperature in the inlet plane 0. The injector body has been produced by means of SLM (Selective Laser Melting) to allow the realization of its complex shape.

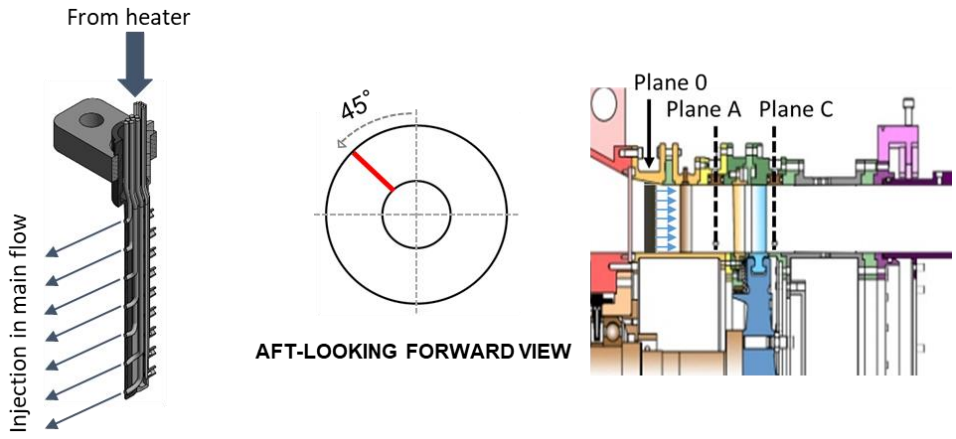

Figure 2: Cross section of the air injector and detailed view of the stage and circumferential position of the temperature inlet distortion generator.

Table 3: Details of the T distortion injected air configurations.

Mass flow [g/s]	Temperature [K] ([°C])					
2	298 (25)	310.5 (37.5)	323 (50)	363 (90)	368 (95)	373 (100)
2.5	298 (25)	310.5 (37.5)	323 (50)	363 (90)	-	-

Different temperature distortions were obtained injecting air through the injector mounted in plane 0, 2.4 IGV chords upstream of the IGV, as depicted in Figure 2. Different mass flows and temperatures were tested. Table 3 resumes all the tested configurations.

Air Supply Line

In order to provide a stable supply of air to be injected, an air-supply and heating system was designed and built. A scheme of the system is presented in Figure 3. The air flows from the lab compressed line into a filter fitted with a pressure regulation valve before encountering the fine regulation valve, used to precisely set the mass flow needed for the desired inlet temperature distortion. Subsequently, the temperature, pressure and mass flow are measured (mass flow meter Omega FMA 1600). The air then enters the heater used to regulate the injection temperature (Omega AHPF-062 with 400 W - 240 V). The thermocouple used for the regulation of the injection air temperature is fitted at the exit of the heater. The air flow is divided in four pipes of the same length and the temperature is measured right upstream of the injectors, in order to guarantee the same mass flow and temperature in each injector.

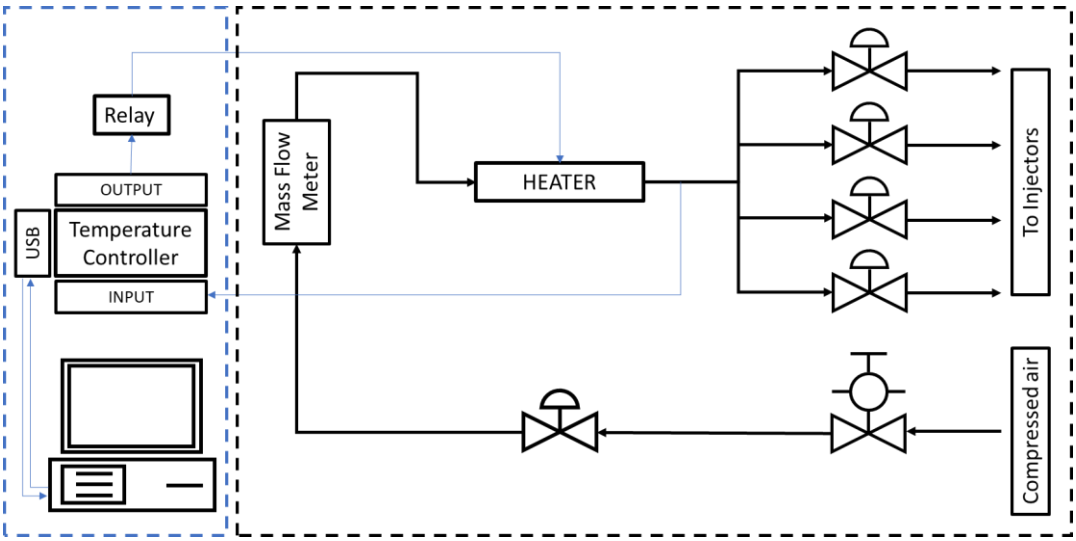

Figure 3: Full scheme of the air supply and of the control system.

The regulation of the air temperature is achieved with a PID controller. The brain of the regulation system is the temperature controller "Omega CN32PT-145". The temperature at the exit of the heater was measured with a thermocouple and the signal was used as input of the controller loop. The output control signal from the controller was directed to a relay, responsible to pilot the power supply of the air heater. Furthermore, the temperature controller was connected to the regulation software running on the control-PC, in order to remotely adjust the temperature of the air supply.

Measurements setup

Different measurement techniques were applied to study both the flow field and the vibrations of the rotor blades. Steady aerodynamic measurements were carried out downstream of the LPT stage and the rotor blade vibrations were acquired by means of strain gauges. In the following paragraphs the complete details of the measurement methodology will be described.

Aerodynamic measurements

Steady aerodynamic measurements upstream of the LPT stage were carried out by means of five-hole-probe. The probe has a head with a diameter of 2.5 mm and a picture is shown in Figure 4. The calibration range is shown in Table 4, where negative values of the yaw angle indicate a counter-rotating flow and negative values of pitch angle indicate the flow pointing towards the hub. Additionally, Table 4 shows also the measurement uncertainties (within a 95% confidence interval) of the five-hole-probe measurements, which include the error due to the approximation, random error and the systematic error of the pressure transducers.

Figure 4: Detail of the five-hole-probe head and position of the measurement sectors upstream (plane A) of the LPT stage.

The measurements were carried out upstream of the LPT stage in Plane A 1.5 IGV chords downstream of the inlet guide vanes. The position of the measurement plane is highlighted in Figure 2. The sampled angular sector covered 5.4 IGV pitches and 6.2 stator pitches and about 95% of the span. The sketch in Figure 4 shows the relative position between the measurement sectors in plane A and the distortion injector, represented by the black dashed line. Traversing was done along radial lines. At each measurement point the probe was rotated in the flow direction to reach the highest accuracy and to ensure to be within the calibration range.

Table 4: Measurement uncertainties and calibration range of the five-hole-probe.

Measurement uncertainties			
Ma	+0.006	-0.003	[-]
α	+0.5	-0.08	[deg]
Pt	+3.3	-3.0	[mbar]
P	+5.3	-5.2	[mbar]
Calibration range			
	Minimum	**Maximum**	**Step**
Ma	0.1	0.8	0.1
α	-20	20	4
γ	-20	20	4

Blade Vibrations measurements

The rotor blades vibrations were measured with strain gauges applied on 12 different blades. The sensors were applied on the blades accordingly to (Schönleitner, et al., 2015). It is necessary to state that in this work only the results obtained from the analysis of one representative strain gauge (SG2) will be described. A picture of the strain gauges applied on the rotor blades is presented in Figure 5.

The strain gauges' resistance is 350Ω +/-0.30% with a gauge factor of 2.05+/- 1.0%, a transverse sensitivity of 0.0% and a temperature coefficient of gauge factor of 101 +/-10 [10-6/K].

A telemetry system able to operate at a rotational speed up to 11000 rpm and temperatures up to 150 °C and to acquire data at a maximum sample rate of 400 kSamples/s was employed in combination with the strain gauges. During the measurements, the strain gauge signals were transmitted via antenna and acquired using a high-accuracy data acquisition module with a sampling rate of up to 204800 samples/s. The data were then transmitted to a PC via optic-fibre-cabling.

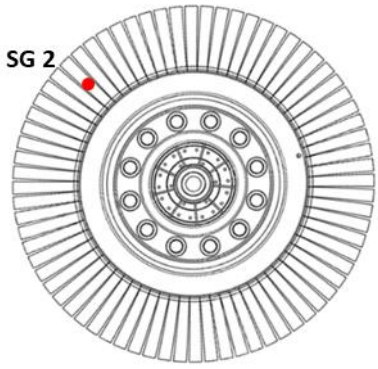

Figure 5: Strain gauges applied on the rotor blades and position of SG2.

RESULTS

Aerodynamic results

The results of the investigation carried out by means of 5HP in plane A are presented in the following paragraphs. The most relevant tested configurations are collected in the contour plots of total temperature, in order to highlight the effect of the air injection on the total temperature field at the inlet of the LPT stage. Firstly, the clean inlet conditions will be presented, to set the reference for the following comparisons. Then the total pressure and total temperature radial profiles measured in plane A will be described in order to study the influence of the secondary air injection on the LPT stage inlet conditions.

Clean inflow

Firstly, the total pressure and total temperature contours in plane A are presented in Figure 6. As can be observed in the total pressure contour plot shown in Figure 6 (a), the flow field upstream of the LPT is not uniform and three main effect can be identified. Since the IGVs are mounted on the outer casing leaving a 0.5 mm gap at the hub, the generation of a leakage vortex is allowed. The presence of this vortex is the cause of the region of low total pressure near the hub, identified in the picture with the letter B. The wakes generated by the vanes prevail in the region between 10% and 90% of the passage and are marked with black dashed lines. As a consequence of the circumferential swirl determined by the flow angle at the exit of the IGV, the wakes are bent towards the outer casing. In the upper passage section, lobes of low total pressure are created by the upper passage vortices present in the casing region of the IGV. Letter A is superimposed to the plot in the figure in order to highlight these structures.

The temperature distribution (plot (b) in Figure 6) appears to be almost constant in the lower part of the channel, with the exception of a limited lower total temperature region in the lower-right corner of the measured sector, highlighted with the letter C in the figure. The effect of the secondary vortices generated by the inlet guide vanes positioned upstream of the measurement plane can be recognised in a band of higher temperature located in the upper region of the channel (A'). This band is spatially partitioned according to the number of IGV present in the area corresponding to the measurement sector.

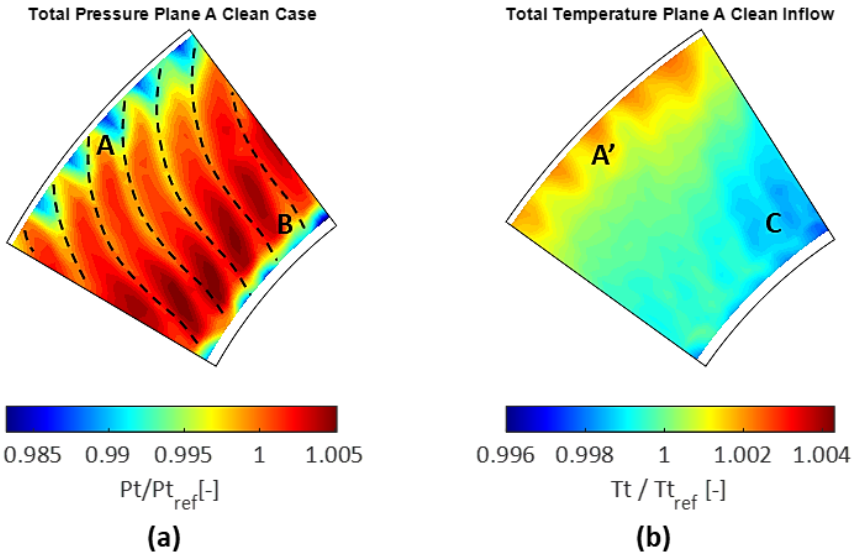

Figure 6: Distributions of total pressure (a) and total temperature (b) in plane A for the reference case.

Inlet Distortion Cases

The total temperature contour plots obtained for the two injected mass flow cases are depicted in Figure 7 in order to highlight the effect of the air injection temperature and mass flow on the LPT inlet and define the main characteristics of the temperature distortion. In this figure only the plots relative to the most representative temperatures of the injected air are reported. In particular, the cases shown in Figure 7 are: $T_j = 37.5\ °C$ (a) and $T_j = 100\ °C$ (b) for the 2.0 g/s injected mass flow and $T_j = 37.5\ °C$ (c) and $T_j = 90\ °C$ (d) for the 2.5 g/s injected mass flow.

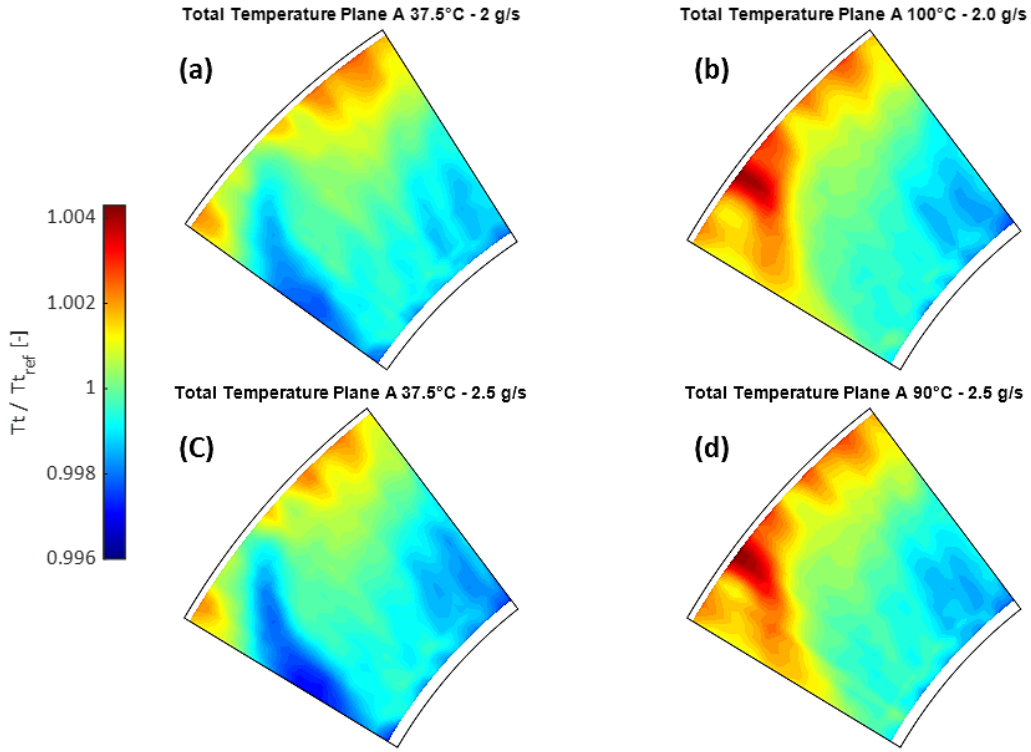

Figure 7: Total temperature distributions in plane A. (a) 2.0 g/s injection case 37.5 °C; (b) 2.0 g/s injection case 100 °C; (c) 2.5 g/s injection case 37.5 °C; (d) 2.5 g/s injection case 90 °C.

Observing the plots, it is possible to identify the effect of the injection of air on the inlet flow of the turbine stage. Both the cold air injection and the hot air injection create a distinct and well recognizable region of colder or warmer temperature in the field respectively. The intensity of the inhomogeneity appears to depend on the injected mass flow and on the temperature of the injection and to interest almost two IGV passages.

Regarding the position of the temperature distortion, the colder flow is more evident in lower half of the passage, whereas the higher temperature injection appears to have a stronger impact on the upper section of the passage. This could be due to the interaction between the injected air and the vanes, in particular with the upper passage vortex already presented in Figure 6. Moreover, the effect of the IGVs wakes is recognizable in the skewed shape that the temperature distortion assumes after passing through them.

In all injection cases, the total temperature distortion travels from the injection plane (plane 0) to the measurement plane (plane A), through the IGV and is still well recognisable. It is possible to directly link the extent the temperature difference to the injected mass flow, as can be observed comparing the plots relative to a $T_j = 37.5\ °C$. The distortion reaches a temperature difference up to 75% of the reference range in the $\dot{m}_j = 2.5\ g/s$ case (Figure 7 (c)) and is more intense than in the $\dot{m}_j = 2.0\ g/s$ case Figure 7 (a)) in which it only reaches a maximum temperature difference of 65% of the reference temperature range. The distortion, and in particular the intensity of the region with different temperature will be connected in the following sections to a variation of the rotor blade vibration amplitudes.

In order to provide an additional visualisation of the effect of the circumferential inlet air injection on the total pressure and temperature field in plane A, the circumferentially mass averaged spanwise distributions of both total pressure and total temperature fields is plotted in Figure 8. The two plots on the left (a) represent the $\dot{m}_j = 2.0\ g/s$ case , while the plots on the right (b) refer to the $\dot{m}_j = 2.5\ g/s$ injection case. In both cases the values are normalised with the average temperature and pressure measured for the clean inflow case.

Regarding the lower mass flow case, the trend of the temperature distributions follows accurately the temperature of the injected air, determining a colder total temperature distribution for the 37.5°C case and hotter temperature profiles for the cases 95°C 100°C. Since the injected air temperature difference between the two last cases is only 5 °C, these temperature profiles result very similar. Observing the colder air case temperature distribution, one can note that the lower temperature air injection determines a modification in the temperature profile particularly in the lower half of the channel, while the effect of the warmer air injection is stronger at higher span. Contrarily to the temperature distributions, the pressure profiles are very similar, indicating that the secondary air injection system and injectors developed do not influence the stage inlet total pressure and that only an inlet temperature distortion is generated with this specific injected mass flow.

Observing the $\dot{m}_j = 2.5\ g/s$ case pressure distribution, a very similar trend of total pressure in plane A can be recognised. Nevertheless, the injection of a higher mass flow causes a slightly higher total pressure localised in two small regions at around 80% and 20% span. It must be considered that these differences are very small and can therefore be neglected as this would not cause a noticeable modification in the operation of the turbine. By studying the graph showing the temperature profiles it can be seen that also in this case the temperature profiles follow the trend of the injected air temperature, determining a colder total temperature distribution for the 25°C, 37.5°C 50°C injection temperatures and warmer temperature profiles for the 90°C case. Moreover, the higher injected mass flow causes a stronger influence of the injection on the total temperature profiles. In particular, the colder air cases seem to have a more intense effect on the temperature distribution along the whole span and not only in the lower passage region as it was case for the $\dot{m}_j = 2.0\ g/s$ case. Despite that, the hotter air injection results still stronger at higher span. The temperature difference in the tip region of plane A can be connected to a difference of stage inlet flow angles. According to (Kerrebrock & Mikolajczak, 1970) the direction of the relative velocity at the stage inlet, and consequently at the rotor inlet, differs according to the increased or decreased temperature in the distorted region.

Differences of inlet flow angle are responsible for changes in the behaviour of the tip leakage flow, as suggested by (Coull & Atkins, 2015), and consequently have an influence on the rotor blade vibratory excitation in that region.

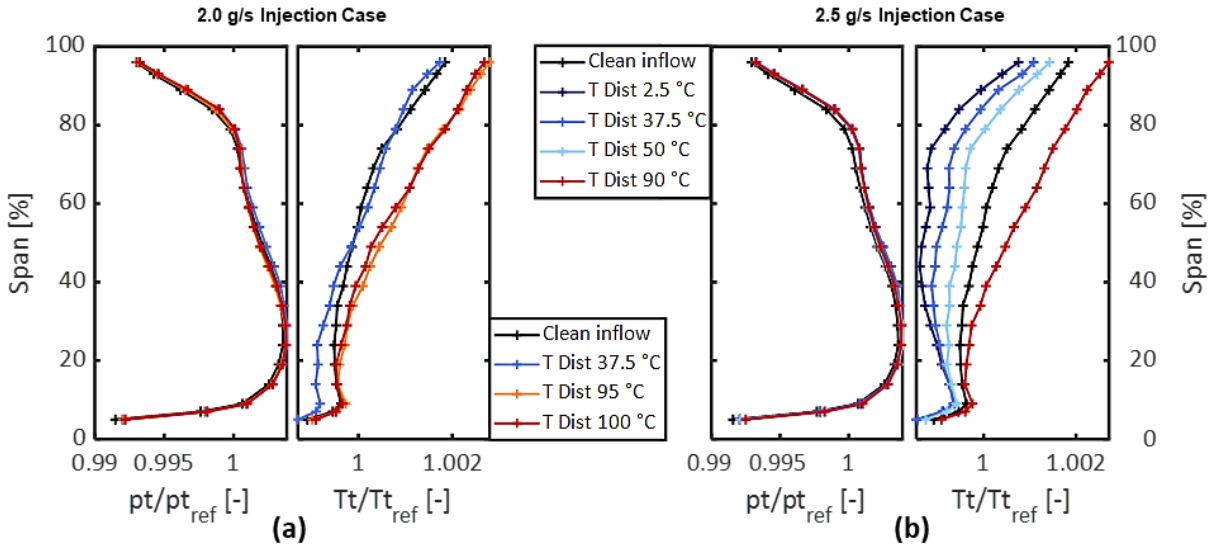

Figure 8: Radial distributions of circumferentially mass averaged total pressure and temperature for the two injection mass flows. (a) 2.0 g/s injection case; (b) 2.5 g/s injection case.

Combining the information obtained from all the aerodynamic results presented in this section it is possible to conclude that the mass flow and the temperature of the injected air have a strong effect on the resulting total temperature distortion at the LPT stage inlet. In particular, two effects can be highlighted. Firstly, it is evident that the higher is the injected mass flow, the higher is the intensity of the distortion obtained in plane A. Secondly, the total temperature distortion amplitude seems to follow a quite linear relation with the injection temperature. However, it should be noted that the injection of warmer air behaves differently from the injection of colder air, resulting in a different absolute amplitude of the distortion due to the same (negative or positive) difference between the main flow and injected air temperatures. This can be understood observing the temperature profiles in Figure 8 (b): the amplitude of the distortion for case 90 °C is higher than the distortion obtained for case 50 °C, even though the absolute temperature difference between the injected air and the main flow is higher for the second case. This results could be connected to a different mixing behaviour of high temperature, and therefore low density, air injected in the colder main flow, compared to the injection of lower temperature and higher density fluid in warmer air.

Blade vibration results

The blades vibrations frequency spectra will be presented in the following section to analyse the impact of the inlet temperature distortion on the rotor blade vibratory response. The strain gauge data were averaged with respect to the rotational speed and then FFT was performed. The spectra obtained have a resulting frequency resolution of 5 Hz, which is considered sufficient for this study. All the results presented in this work are relative to one strain gauge (SG2).

Figure 9 shows a comparison of the spectra obtained from the signals measured from a single strain gauge. The results are presented in the form of strain normalised over the amplitude of the first eigenfrequency of the reference case. A comparison between the spectra obtained for the reference case (a), the $\dot{m}_j = 2.0\ g/s$ (b) and the $\dot{m}_j = 2.5\ g/s$ (c) enables the recognition of the impact of the distortion and in particular of the temperature and of the mass flow of the injected air on the rotor blade vibrations.

Observing the reference case plot in Figure 9 (a), it is possible to identify the characteristics of the first six vibratory modes and the excitation determined by the stator vanes. More specifically, the

highest peak in the spectrum is related to the first eigenfrequency (1st flap-wise bending mode), located around 940 Hz. This mode will be used as major element for the comparison between the examined cases. Complete details about the rotor blades modes were presented in (Schönleitner, et al., 2015)

As it was presented in (Simonassi, et al., 2020), a modification of the vibratory response of the first eigenfrequency is determined by the amplification of the aerodynamic excitation at low engine orders originating from the spatial non-uniformity in the distorted region. Specifically, by comparing the plots relative to the distorted cases (a) and (b) one can derive the impact of the temperature of the distortion. In particular, the amplitude of the first mode obtained for the colder air injection cases (T_j = 37.5°C) is lower than the level of the EF1 measured for the clean inflow configuration. The EF1 amplitude measured for the T_j = 37.5°C - $\dot{m}_j = 2.0\ g/s$ case is approximately 85% of the EF1 amplitude of the reference case, while in the T_j = 37.5°C - $\dot{m}_j = 2.5\ g/s$ configuration the first vibratory mode amplitude resulted lower than 70% of the reference value. On the contrary, both the EF1 amplitudes measured with an inlet non-uniformity characterised by a profile of hotter air are higher than the amplitude of the reference case. Namely, the T_j = 100°C - $\dot{m}_j = 2.0\ g/s$ amplitude amounted to approximately 170% of the reference case value and the T_j = 90°C - $\dot{m}_j = 2.5\ g/s$ configuration showed an amplitude up to more than 110% of the clean case intensity. Consequently, since a very similar trend was shown by the two injection mass flows tested, the distorted temperature inflow conditions are thought to influence the rotor blades excitation according to the temperature in the distorted flow region.

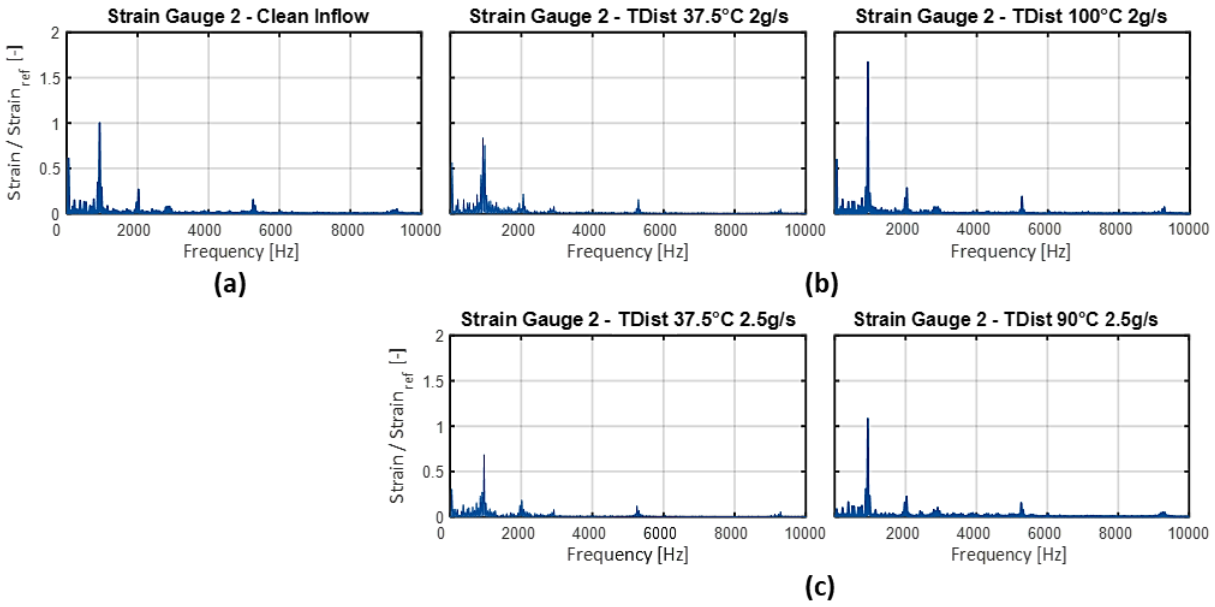

Figure 9: Forced response spectra of strain gauge 2. Clean reference case (a); 2 g/s injection case (b); 2.5 g/s injection case (c).

In order to analyse the relationship between the temperature of the inflow distortion and the blades vibrations, the amplitudes of the EF1 are plotted in Figure 10 for the $\dot{m}_j = 2.0\ g/s$ (a) and $\dot{m}_j = 2.5\ g/s$ (b) cases respectively. This visualisation allows the understanding of the relationship between inlet distortion temperature and blade vibrations amplitudes. In particular, there seems to be a direct relation between the two, so that the hotter the air injected the higher the EF1 amplitude. The effect of the temperature on the aerodynamic damping could be connected this result. In particular, the region of the passage characterised by a hotter temperature determines a higher forced response of the rotor blades as they cross the distorted flow. The opposite was measured for the colder air injection

cases. A possible explanation could be found considering that the major differences between the temperature profiles were found in the tip region, where aerodynamic effects are associated with major changes in the rotor blades vibratory response. Similarly to what observed by (Ioannou & Sayma, 2017) and (Ioannou, 2015), the temperature excess, or defect, present in the region characterised by the flow distortion determines a variation of the energy flux impinging on the rotor blades, in particular in the tip region. This means that for the $T_j > T_{0,avg}$ cases there is a higher concentration of highly energetic fluid at high span, while in the $T_j < T_{0,avg}$ cases the energy of the fluid available in the distorted region is lower. Therefore, this excess or defect of energy in the inlet distortion, could be linked to higher or lower blade vibratory response respectively.

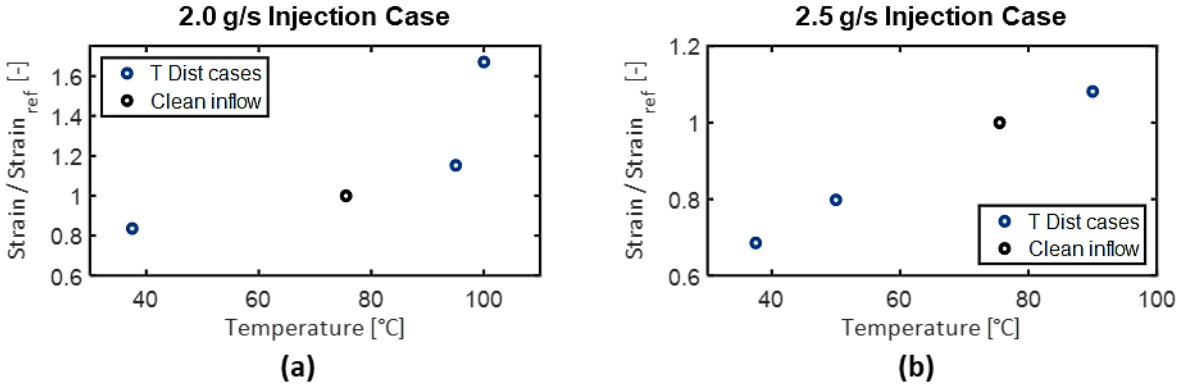

Figure 10: EF1 amplitudes for different inlet distortion temperatures. 2 g/s injection case (a); 2.5 g/s injection case (b).

CONCLUSION

Air injection at the inlet of a 1.5 stages low pressure test turbine was used to generate a circumferential total temperature distortion in the inflow of the LPT stage. Aerodynamic and vibration measurements were carried out at engine relevant operating conditions in order to study the influence of the distortions on the aerodynamic and vibratory performance of the turbine. The air needed to produce the non-uniformity in the inflow was supplied to an injector by a supply line equipped with an air heater and a temperature control system. This setup permitted to vary the mass flow and temperature of the injected air, allowing the investigation of multitude of different temperature distortion intensities.

Five-hole-probe measurements were carried out to study the stage inlet flow field, allowing the description of the non-uniform temperature circumferential distribution and the effects of the injection on the other aerodynamic quantities, in particular the inlet total pressure and flow angle. The different injection cases were analysed and the main differences that characterise the distorted flow region depending on the mass flow and temperature of the injected air were discussed.

The blades forced response was acquired at the nominal operating point by means of strain gauges applied on the blades surfaces, in combination with a telemetry system. The vibrations data seem to highlight a direct relationship between inlet temperature distortion and blade vibrations amplitudes. In particular, the injection of warmer air determines a higher rotor blade forced response amplitude, whereas a temperature of the injected air colder than the temperature of the main flow could be liked to lower rotor blade vibratory response. This direct effect of the temperature of the inlet distortion on the first eigenfrequency amplitude could be connected to a modification of the aerodynamic forcing on the rotor blades determined by the variation of the flow energy impinging on the rotor blades driven by the temperature distortion.

To conclude, the alterations created by temperature non-uniformities in the stage inlet flow field and the modifications of the rotor vibration characteristics were investigated. The specific influence on the LPT stage aerodynamics and vibrations of the temperature distortion temperature and

amplitude was also examined. Ultimately, this study provided insights on the effect on temperature distortion on localised changes of aerodynamic damping and their direct effect on the rotor blade vibrations.

REFERENCES

Breard, C., Green, J. & Imregun, M., 2003. Low-engine-order excitation mechanisms in axial-flow turbomachinery. *Journal of Propulsion and Power,* Volume 19, pp. 704-712.

Butler, T. L., Sharma, O. P., Joslyn, H. D. & Dring, R. P., 1989. Redistribution of an inlet temperature distortion in an axial flow turbine stage. *Journal of Propulsion and Power,* 5(1), pp. 64-71.

Coull, J. D. & Atkins, N. R., 2015. The Influence of Boundary Conditios on TIp Leakage Flow. *J. Turbomach.,* 137(6).

Gaetani, P. et al., 2019. Computational and Experimental Study of Hot Streak Transport Within the First Stage of a Gas Turbine. *J. Turbomach.,* 142(8), p. 081002.

Hermanson, K. S. & Thole, K. A., 2002. Effect of nonuniform inlet conditions on endwall secondary flows. *J. of Turbomach.,* 124(4), pp. 6223-631.

Ioannou, E., 2015. *The effects of temperature distortion on aerodynamics and low engine order forced response in axial turbines,* s.l.: City University London.

Ioannou, E. & Sayma, A., 2017. Full anulus numerical study of hot streaks propagation in a hydrogen-rich synges fired heavy duty axial turbine. *J. Power and Energy,* 231(5), pp. 344-356.

Kerrebrock, J. L. & Mikolajczak, A. A., 1970. Intra-stator transport of rotor wakes and its effect on compressor performance. *Journal of Engineering for Power,* 92(4), pp. 359-368.

Lakshminarayana, B., 1975. Effects of inlet temperature-gradients on turbomachinery performance. *Journal of Engineering for Power,* 97(1975), pp. 61-74.

Manwaring, S. & Kirkeng, K. L., 1997. *Forced response vibrations of a low pressure turbine due to circumferential temperature distortions.* Stockholm, Proceedings of the 8th International Symposium on Unsteady Aerodynamics and Aeroelasticity of Turbomachines.

Moser, M., Kahl, G., Kulhanek, G. & Heitmeir, F., 2007. *Construction of a Subsonic Test Turbine Facility for Experimental Investigations of Sound Generation and Propagation for Low Pressure Turbines.* Beijing, ISABE Conference 2007.

Munk, M. & Prim, R., 1947. *On the multiplicity of steady gas flows having the same streamline pattern.* s.l., Proceedings of the National Academy of Sciences of the United States of America.

Ong, J. & Miller, R. J., 2012. Hot Streak and Vane Coolant Migration in a Downstream Rotor. *ASME J. Turbomach.,* Volume 134, p. 051002.

Schönleitner, F., Traussnig, L., Marn, A. & Heitmeir, F., 2015. *Modal Characterization, Strain Gauge Setup and 1-Way FSI of a Low Pressure Turbine Rotor Blading.* Montreal

Schwab, J. R., Stabe, R. G. & Whitney, W. J., 1983. Analytical and experimental study of flow through an axial turbine stage with a nonuniform inlet radial temperature profile. *AIAA Journal.*

Simonassi, L. et al., 2019. *Aeroelastic and Aerodynamic Investigation of a Low Pressure Turbine Under the Influence of a Circumferential Inlet Distortion.* Phoenix.

Simonassi, L. et al., 2020. *Eperimental Study on the Efefct of Clocking on the Propagation of Inflow Pressure Distortion in a Low Pressure Turbine.* Lodon, ASME Turbo Expo 2020.